

## A High-Resolution Non-Detection of Escaping Helium In The Ultra-Hot Neptune LTT 9779b: Evidence for Weakened Evaporation

SHREYAS VISSAPRAGADA,<sup>1,\*</sup> PATRICK MCCREERY,<sup>2</sup> LEONARDO A. DOS SANTOS,<sup>3</sup> NÉSTOR ESPINOZA,<sup>3</sup>  
ANDREW MCWILLIAM,<sup>4</sup> NORIYUKI MATSUNAGA,<sup>5,6</sup> JÉA ADAMS REDAI,<sup>1</sup> PATRICK BEHR,<sup>7,8</sup> KEVIN FRANCE,<sup>7,8</sup>  
SATOSHI HAMANO,<sup>9</sup> CHARLIE HULL,<sup>4</sup> YUJI IKEDA,<sup>10,6</sup> HARUKI KATOH,<sup>6</sup> HIDEYO KAWAKITA,<sup>6,11</sup>  
MERCEDES LÓPEZ-MORALES,<sup>1</sup> KEVIN N. ORTIZ CEBALLOS,<sup>1</sup> SHOGO OTSUBO,<sup>6</sup> YUKI SARUGAKU,<sup>6</sup> AND TOMOMI TAKEUCHI<sup>6</sup>

<sup>1</sup>Center for Astrophysics | Harvard & Smithsonian, 60 Garden Street, Cambridge, MA 02138, USA

<sup>2</sup>Department of Physics and Astronomy, Johns Hopkins University, 3400 N Charles St, Baltimore, MD 21218, USA

<sup>3</sup>Space Telescope Science Institute, 3700 San Martin Drive, Baltimore, MD 21218, USA

<sup>4</sup>The Observatories of the Carnegie Institution for Science, 813 Santa Barbara Street, Pasadena, CA 91101

<sup>5</sup>Department of Astronomy, School of Science, The University of Tokyo, 7-3-1 Hongo, Bunkyo-ku, Tokyo 113-0033, Japan

<sup>6</sup>Laboratory of Infrared High-resolution spectroscopy (LiH), Koyama Astronomical Observatory, Kyoto Sangyo University, Motoyama, Kamigamo, Kita-ku, Kyoto, 603-8555, Japan

<sup>7</sup>Department of Astrophysical & Planetary Sciences, University of Colorado Boulder, Boulder, CO, 80309, USA

<sup>8</sup>Laboratory for Atmospheric and Space Physics, University of Colorado Boulder, Boulder, CO, 80303, USA

<sup>9</sup>National Astronomical Observatory of Japan, 2-21-1 Osawa, Mitaka, Tokyo 181-8588, Japan

<sup>10</sup>Photocoding, 460-102 Iwakura-Nakamachi, Sakyo-ku, Kyoto 606-0025, Japan

<sup>11</sup>Department of Astrophysics and Atmospheric Sciences, Faculty of Science, Kyoto Sangyo University, Motoyama, Kamigamo, Kita-ku, Kyoto 603-8555, Japan

### ABSTRACT

The recent discovery of “ultra-hot” ( $P < 1$  day) Neptunes has come as a surprise: some of these planets have managed to retain gaseous envelopes despite being close enough to their host stars to trigger strong photoevaporation and/or Roche lobe overflow. Here, we investigate atmospheric escape in LTT 9779b, an ultra-hot Neptune with a volatile-rich envelope. We observed two transits of this planet using the newly-commissioned WINERED spectrograph ( $R \sim 68,000$ ) on the 6.5 m Clay/Magellan II Telescope, aiming to detect an extended upper atmosphere in the He 10830 Å triplet. We found no detectable planetary absorption: in a 0.75 Å passband centered on the triplet, we set a  $2\sigma$  upper limit of 0.12% ( $\delta R_p/H < 14$ ) and a  $3\sigma$  upper limit of 0.20% ( $\delta R_p/H < 22$ ). Using a H/He isothermal Parker wind model, we found corresponding 95% and 99.7% upper limits on the planetary mass-loss rate of  $\dot{M} < 10^{10.03}$  g s<sup>-1</sup> and  $\dot{M} < 10^{11.11}$  g s<sup>-1</sup> respectively, smaller than predicted by outflow models even considering the weak stellar XUV emission. The low evaporation rate is plausibly explained by a metal-rich envelope, which would decrease the atmospheric scale height and increase the cooling rate of the outflow. This hypothesis is imminently testable: if metals commonly weaken planetary outflows, then we expect that *JWST* will find high atmospheric metallicities for small planets that have evaded detection in He 10830 Å.

### 1. INTRODUCTION

Ultra-hot Neptunes are an enigmatic new part of exoplanet population. Prior to the launch of the *Transiting Exoplanet Survey Satellite* (*TESS*) mission, there were no Neptune-mass planets known with orbital periods of less than a day, despite our ability to detect them.

The dearth of ultra-hot Neptunes has been variously attributed to tidal disruption during high-eccentricity migration, photoevaporation, and/or Roche-lobe overflow (Kurokawa & Nakamoto 2014; Matsakos & Königl 2016; Mazeh et al. 2016; Owen & Lai 2018; Ionov et al. 2018; Koskinen et al. 2022; Thorngren et al. 2023). Over the past few years, *TESS* has revealed that the Neptune desert is not empty (Jenkins et al. 2020; Armstrong et al. 2020; Persson et al. 2022; Naponiello et al. 2023; Osborn et al. 2023). Studying the properties of desert-dwelling planets may help us understand the physical

Corresponding author: Shreyas Vissapragada  
shreyas.vissapragada@cfa.harvard.edu

\* 51 Pegasi b Fellow

mechanisms that clear out the Neptune desert and drive the evolution of short-period exoplanets.

LTT 9779b was the first ultra-hot Neptune to be unveiled by *TESS*. At  $M_p = 29.32^{+0.78}_{-0.81} M_\oplus$  and  $R_p = 4.72 \pm 0.23 R_\oplus$ , the planet has a density of just  $\rho_p = 1.54 \pm 0.12 \text{ g cm}^{-3}$  (Jenkins et al. 2020). It therefore appears to be volatile-rich despite remarkable proximity ( $P = 0.79 \text{ d}$ ,  $a = 0.017 \text{ au}$ ) to a G7V host star. LTT 9779b’s orbital separation is only  $1.5\times$  the Roche limit for an incompressible fluid  $a_{\text{Roche}} = 2.44 R_\star (\rho_\star / \rho_p)^{1/3}$ , so it may be tidally distorted as well. For planets at LTT 9779b’s orbital distance, Koskinen et al. (2022) predict the 1 bar substellar radius to be  $\sim 5\%$  larger than the polar radius for hot Jupiter and hot Neptune analogs (see also e.g. Li et al. 2010; Rappaport et al. 2013; Delrez et al. 2016).

This planet is a compelling target for atmospheric spectroscopy, especially for studies of atmospheric erosion. Assuming the envelope composition is dominated by  $\text{H}_2/\text{He}$  ( $\mu = 2.3 \text{ amu}$ ), the scale height of LTT 9779b’s atmosphere at  $R_p$  is 550 km, similar to many hot Jupiters that have been studied with *HST* and *JWST*. Also, the planet has a restricted Jeans parameter  $\Lambda = GM_p m_{\text{H}} / (k_{\text{B}} T_{\text{eq}} R_p) \approx 27$ , a gravitational potential  $\Phi = GM_p / R_p \approx 4 \times 10^{12} \text{ erg g}^{-1}$ , and a Roche lobe filling factor  $R_p / R_{\text{Roche}} \approx 50\%$  (Eggleton 1983). Photoevaporation and/or Roche lobe overflow should be vigorous for a planet so close to its host star with such low  $\rho_p$ ,  $\Lambda$ ,  $\Phi$ , and  $R_{\text{Roche}}$  (Salz et al. 2016; Kubyshkina et al. 2018; Caldiroli et al. 2022; Edwards et al. 2023). In fact, escaping atmospheres have been detected for many Jupiter- and Neptune-sized planets with similarly small  $\rho_p$ ,  $\Lambda$ ,  $\Phi$ , and/or  $R_{\text{Roche}}$  (Dos Santos et al. 2023).

LTT 9779b is therefore an excellent target for transmission spectroscopy in the metastable He 10830 Å triplet, which probes atmospheric escape (Oklopčić & Hirata 2018; Spake et al. 2018). Planets orbiting stars cooler than the Sun (Oklopčić 2019) are now routinely studied in He 10830 Å, allowing for population-level constraints on planetary mass-loss rates (Vissapragada et al. 2022; Allart et al. 2023; Guilluy et al. 2023; Dos Santos et al. 2023). Models suggest that planets orbiting late G stars like LTT 9779 should be favorable targets for helium outflow observations (Oklopčić 2019; Wang & Dai 2021; Biassoni et al. 2023), but there have been relatively few He 10830 Å studies for planets orbiting G-type stars (Allart et al. 2023; Bennett et al. 2023; Guilluy et al. 2023). Recently, Edwards et al. (2023) attempted to constrain helium absorption in the upper atmosphere of LTT 9779b with the *HST* Wide-Field Camera 3 (WFC3) in the G102 grism, but resolving power was ultimately a limiting factor. Using an up-

dated version of the model by Allan & Vidotto (2019), these authors predicted 0.3% absorption in the core of the helium triplet (assuming a 90/10 H/He number ratio), too small to be detected by *HST* WFC3/G102 at  $R \sim 100$ . Ground-based high-resolution spectroscopy can be used to fully resolve the line core, especially in a system as bright as LTT 9779 ( $J = 8.4$ ), but most instruments sensitive to He 10830 Å are located in the northern hemisphere. At a declination of  $-37^\circ$ , LTT 9779b has thus far eluded high-resolution near-infrared transit observations.

Recently, the Warm INfrared Echelle spectrograph to REalize Decent high-resolution spectroscopy (WINERED; Ikeda et al. 2022) was installed on the 6.5 m Clay/Magellan II Telescope to help fill the need for near-infrared high-resolution spectrographs in the southern hemisphere. In this work, we use WINERED to constrain helium absorption in LTT 9779b at high resolving power ( $R \sim 68,000$ ). This is the first time that the WINERED spectrograph has been used to search for helium in an exoplanet atmosphere. In Section 2, we describe our WINERED observations of LTT 9779b as well as our data reduction methodology. We model our He 10830 Å non-detection in Section 3 to constrain the planetary mass-loss rate. Finally, we discuss our findings in Section 4 and conclude in Section 5.

## 2. OBSERVATIONS AND DATA REDUCTION

We observed two transits of LTT 9779b on UT 2023 June 8 and June 12 using the WINERED spectrograph (Ikeda et al. 2016, 2022) on the 6.5 m Clay/Magellan II Telescope at Las Campanas Observatories. Data were obtained in HIRES-Y mode (Otsubo et al. 2016) with the 100  $\mu\text{m}$  slit (slit width  $9''$ ), corresponding to a resolving power of  $R \sim 68,000$ . We took 180 s exposures in an ABBA nod pattern ( $5''$  throw between positions) to correct the OH airglow lines, although for a few strong OH lines we observed some remaining residuals which were later masked. On the first night, we took 64 exposures between UT 06:48 and UT 10:44, covering phases from 0.87 to 0.08 and corresponding to a starting airmass of 1.9 and a final airmass of 1.0. Seeing was excellent throughout the night at around  $0''.5$ . On the second night, conditions were somewhat worse, with the seeing hovering around  $1''.0$ . We took 76 exposures between UT 06:00 and UT 10:22, covering phases from 0.88 to 0.11 and corresponding to a starting airmass of 2.3 and a final airmass of 1.0.

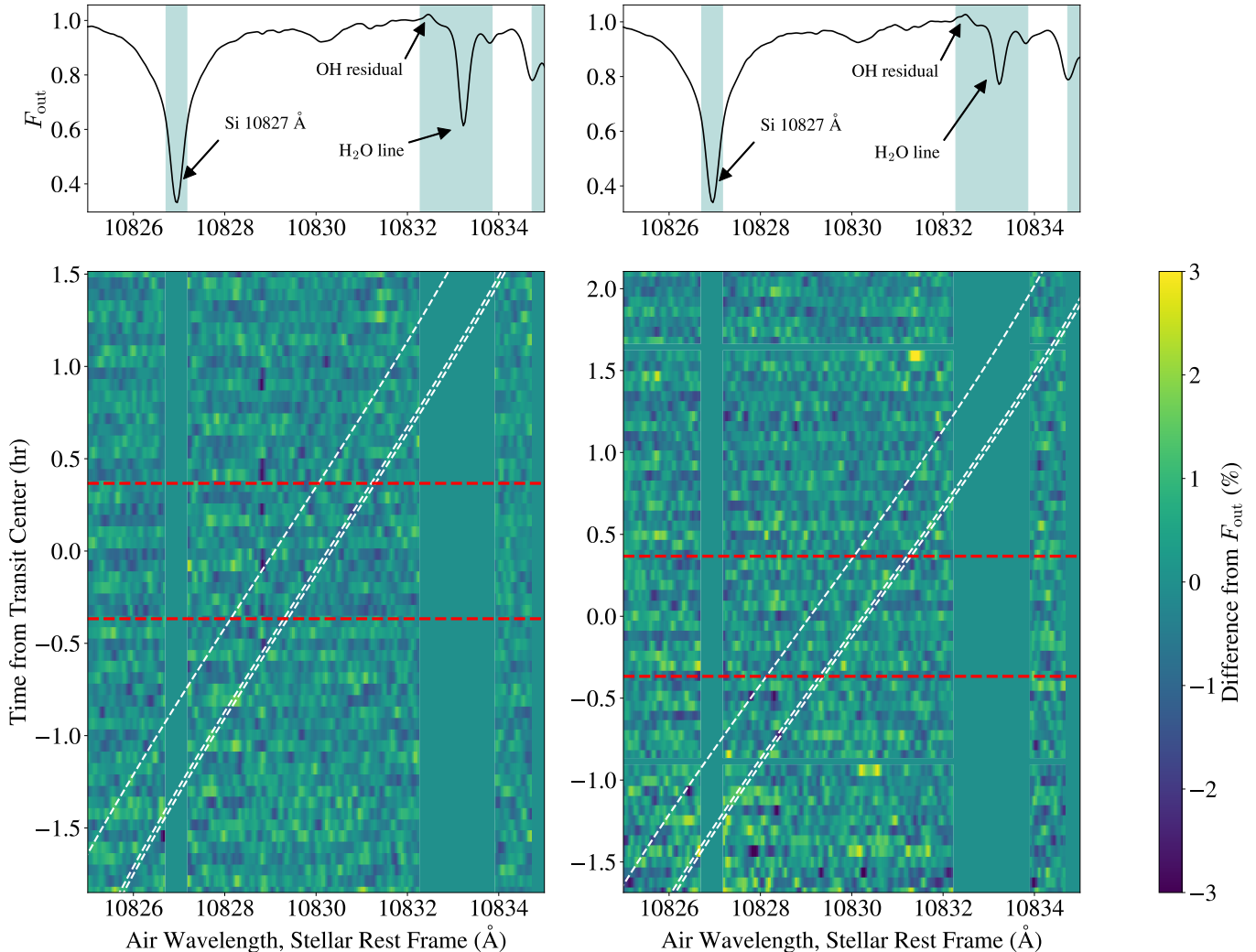


**Figure 1.** Timeseries spectroscopy of LTT 9779 in the stellar rest frame on the first (left) and second (right) nights of data collection. The colors indicate percentage difference from the average out-of-transit spectrum, shown in the upper panel for each night. Red dashed lines indicate the beginning and end of the transit on each night, and the diagonal white lines indicate the positions of the helium triplet lines following the planetary rest frame. The masks for the tellurics and the Si 10827 Å line core are shown with the green vertical bars and annotated in the upper panels, and the two low S/N frames on the second night are indicated by the green horizontal bars.

We reduced the spectra using the WINERED Automatic Reduction Pipeline<sup>1</sup> (WARP ver3.8.12; Hamano et al. in preparation). After flat-fielding and subtracting sky emission and scattered light, WARP performs aperture extraction and wavelength calibration using a ThAr lamp spectrum. We used the fluxes and wavelengths produced by the WARP pipeline for order 163, which includes the helium triplet. On the first night, we obtained a median S/N of 108 and on the second night we obtained a median S/N of 89. Two frames from the

second night were removed due to low S/N < 20 exposures.

We also noticed persistence in our data: when moving from position A to B, a residual trace of about 10% remained at position A, and vice versa. Internal WINERED tests have shown the persistence drops to negligible levels after 30 min, which is longer than the time between subsequent exposures in both of our transit timeseries, and typically longer than the setup time for a given target (meaning that persistence from previous observations of bright stars may affect the first few images). We therefore discarded the first 30 min of data (8 exposures) on each night before performing our analysis, which allowed the residual image from pre-

<sup>1</sup> <https://github.com/SatoshiHamano/WARP>

vious exposures to dissipate and the differential persistence at the A and B positions to stabilize. For future helium observations on WINERED, we advocate including a 30 min on-target overhead period to accommodate the persistence effects.

We proceeded to normalize and align the spectra for timeseries analysis. First, we continuum-normalized the spectra by fitting a fourth-degree Chebyshev polynomial to the line-free regions. We tested using lower-degree polynomials, but found that this increased correlated noise in the final transmission spectrum. Next, we refined the wavelength solution by comparing our spectra to a line-by-line telluric transmission spectrum from HITRAN (calculated with the `hapi` package; Kochanov et al. 2016; Gordon et al. 2022). After accounting for the instrumental broadening with a Gaussian kernel, we cross-correlated the telluric template with the average spectrum on each night. The determined shifts were then corrected to ensure that all data were aligned in the telluric rest frame.

After verifying the wavelength solution, we masked the telluric features for our analysis, following e.g. Orell-Miquel et al. (2022) and Spake et al. (2022). Imperfect telluric correction may introduce extra correlated noise to the final transmission spectrum, which can make it more challenging to estimate a meaningful upper limit in the case of a non-detection. This is especially important when considering the WINERED detector persistence. Telluric absorption and emission may change rapidly even from exposure to exposure, and because the detector has some memory of previous exposures, the observed telluric features for any given exposure are a weighted average over time. We therefore adopt the conservative approach of masking the tellurics near the helium triplet, including water absorption lines and regions with residuals from OH sky subtraction.

Finally, we shifted the data into the stellar rest frame. We used `astropy` to first shift spectra into the Solar System barycenter (SSB) frame, and then shifted into the stellar rest frame using the systemic radial velocity of  $-10.72 \text{ km s}^{-1}$  (Gaia Collaboration et al. 2021) relative to SSB. Before continuing the analysis, we masked the cores of the deep Mg 10811 Å, Si 10827 Å, and Si 10844 Å lines, as we noticed weak ( $\lesssim 1\%$ ) time-correlated variations at these wavelengths. Such residuals are commonly seen and masked in helium observations (e.g. Guilluy et al. 2023; Zhang et al. 2023) and likely originate from the inadequacy of typical spectral extraction approaches for sharp lines in high-SNR data (Zhang et al. 2021).

With these features masked, we constructed a combined out-of-transit stellar spectrum for each night,

shown in Figure 1. Out-of-transit spectra were identified using the linear ephemerides from Edwards et al. (2023), which are precise to better than 30 s for our transits. Each spectroscopic timeseries was then normalized by its combined out-of-transit spectrum to produce the final timeseries spectra. Our final timeseries spectra are shown in Figure 1. No excess helium absorption during transit is evident. To obtain the final planetary transmission spectrum, we shifted these timeseries into the planetary rest frame and took the mean of all the in-transit spectra. The results are shown in Figure 2. The transmission spectrum is noticeably less precise in wavelength bins that are affected by masked tellurics near 10833 Å. Again, no absorption is detected near the 10830 Å triplet in the planetary rest frame.

To set an upper limit on the planetary absorption, we first calculate the mean absorption in a  $0.75 \text{ Å}$  bin centered on the helium triplet ( $-0.04\%$ ), and we take  $\sigma$  to be the rms scatter of the transmission spectrum binned to  $0.75 \text{ Å}$  ( $0.08\%$ ). Estimating  $\sigma$  in this way accounts for correlated noise (Allart et al. 2023; Guilluy et al. 2023). Our resulting  $2\sigma$  and  $3\sigma$  upper limits in a  $0.75 \text{ Å}$  bin centered on the helium triplet are  $0.12\%$  and  $0.20\%$ , respectively. These correspond to 14 and 22 lower-atmospheric scale heights respectively ( $\delta R_p/H < 14$  at  $2\sigma$  and  $\delta R_p/H < 22$  at  $3\sigma$ ), calculated as  $H = \frac{k_B T_{\text{eq}}}{\mu g}$  with  $\mu = 2.3 \text{ amu}$ . Our reporting is slightly different than Allart et al. (2023) and Guilluy et al. (2023), who report  $3\sigma$  for upper limits without the contribution of the mean absorption, and calculate  $H$  assuming  $\mu = 1.3 \text{ amu}$ . Under their assumptions our upper limits are  $0.24\%$  and  $\delta R_p/H < 14$  (the larger  $\delta R_p$  is balanced out by the larger  $H$ , resulting in nearly the same  $\delta R_p/H$  as our  $2\sigma$  upper limit).

### 3. MODELING

We used the open source, one-dimensional, isothermal H+He Parker wind code `p-winds`<sup>2</sup> (Dos Santos et al. 2022) to study the implications of our non-detection for the upper atmosphere of LTT 9779b. As in the original isothermal Parker wind helium models from Oklopčić & Hirata (2018) and Lampón et al. (2020), `p-winds` computes the expected transmission spectrum for the helium triplet in an isothermal wind given an atmospheric escape rate  $\dot{M}$  and an upper atmosphere temperature  $T$  along with an estimate for the top-of-atmosphere XUV spectrum, the H/He number ratio (assumed to be 90/10), well-known planetary parameters like the mass and radius, and the instrumental line spread function

<sup>2</sup> Version 1.4.4 (doi:10.5281/zenodo.7814782). Publicly available in <https://github.com/ladsantos/p-winds>.

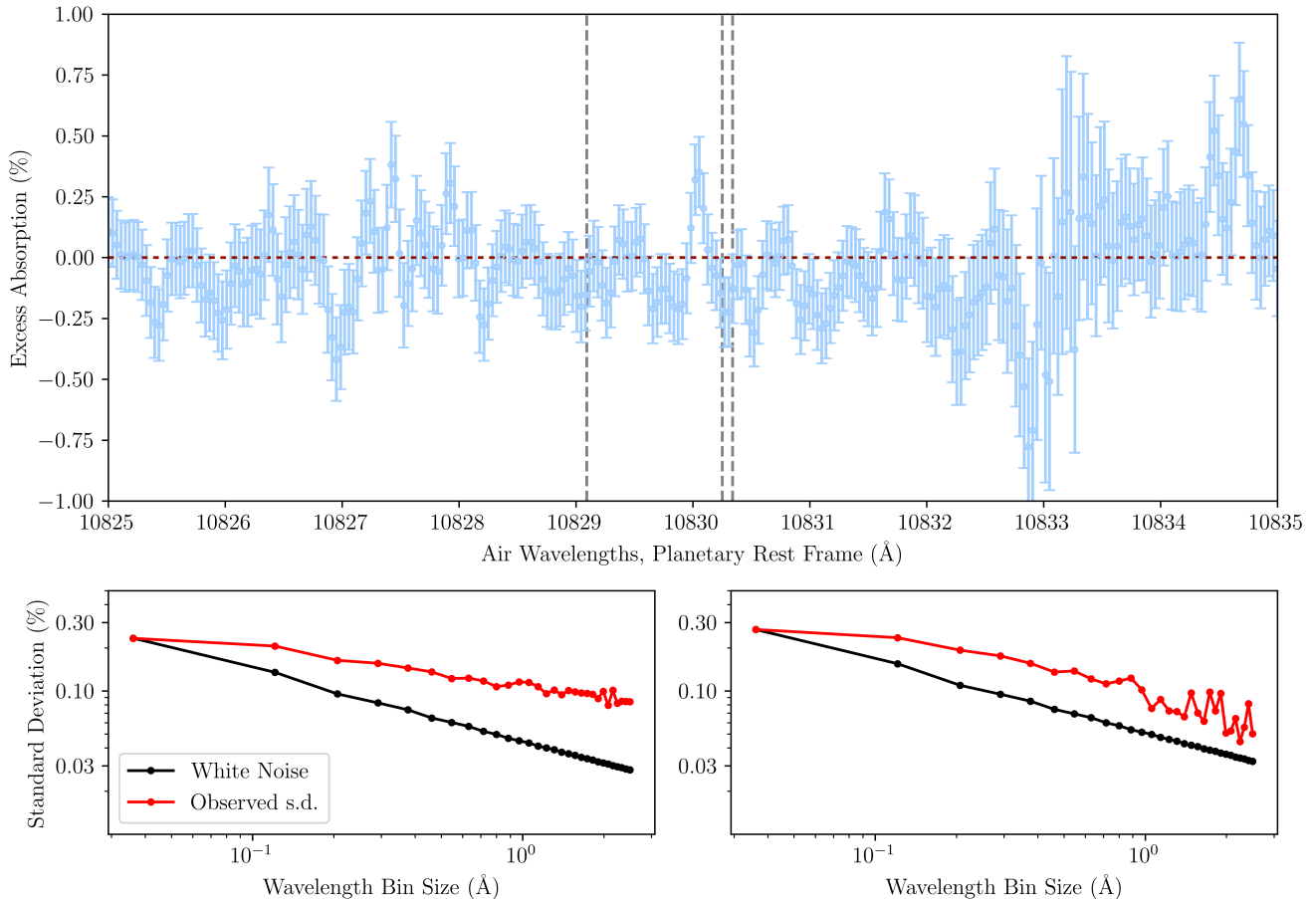


**Figure 2.** Transmission spectrum of LTT 9779b averaged over both nights of observations (top) and Allan deviation plots for night 1 (bottom left) and night 2 (bottom right). In the transmission spectrum, excess absorption in the planetary rest frame is shown with the blue points, and the dashed red curve indicates no excess absorption. The helium triplet wavelength positions are marked with vertical dashed lines, and the increased uncertainty near 10833 Å is due to the masking of telluric features. For visual clarity, the transmission spectrum does not include the  $\beta$  factors that was used to inflate the photon-noise uncertainties during the  $p$ -winds fit. In the bottom panels, the Allan deviation plots show the observed rms of the data as a function of bin size (red) compared to the expectations for white noise (black), indicating a substantial correlated noise component for both nights.

(modeled as a Gaussian with a FWHM of 0.16 Å). Using our observed transmission spectrum in the planetary rest frame, we retrieve posterior probability distributions on  $\dot{M}$  and  $T$ . In the case of our non-detection, we are able to place upper limits on the mass-loss rate.

Our retrieval relies on an estimate for the high-energy spectral energy distribution (SED) of LTT 9779, which is a slowly-rotating ( $v \sin i = 1.06 \pm 0.37 \text{ km s}^{-1}$ ) and relatively inactive ( $\log R'_{HK} = -5.10 \pm 0.04$ ) star (Jenkins et al. 2020). We used the MUSCLES Extension SED for TOI-193/LTT 9779 from Behr et al. (2023). The SED includes a scaled spectrum of the quiet Sun for the X-ray (5 – 100 Å) and FUV (1170 – 2180 Å), as the star was not detected in a 22.9 ks *Chandra*/ACIS-S observation. The stellar EUV (100 – 1170 Å) emission was estimated using the scaling relations from Linsky et al.

(2014). Some FUV emission lines were reconstructed as Gaussian profiles based on the upper limit fluxes from *HST* STIS/G140L data. Lyman- $\alpha$  was reconstructed using the MCMC methods described in Youngblood et al. (2022). The SED includes STIS/G230L data from (2180 – 3110 Å) and STIS/G430L data from (3110 – 5700 Å). A BT-Settl CIFIST stellar model was used for wavelengths 5700 Å and greater.

Before we retrieved posterior probability distributions on our parameters of interest, we needed to account for additional systematic uncertainties arising from correlated noise in the planetary transmission spectrum. Long-wavelength structure is clearly seen in Figure 2. To account for this additional source of uncertainty, we first constructed an Allan deviation plot for each night’s transmission spectrum, calculating the true standard de-



viation of the data at varying wavelength bin sizes ( $\sigma_r$ ) and comparing this to the theoretical expectation for pure photon noise ( $\sigma_w$ ) (Pont et al. 2006; Carter & Winn 2009; Allart et al. 2023). We then inflated the uncertainties on each transmission spectrum by the factor

$$\beta = \sqrt{1 + \left(\frac{\sigma_r}{\sigma_w}\right)^2}, \quad (1)$$

where  $\sigma_r$  and  $\sigma_w$  were estimated at a bin size of  $0.75 \text{ \AA}$ . We found  $\beta = 1.8$  for the first night’s transmission spectrum and  $\beta = 1.7$  for the second night’s transmission spectrum. An approach using Gaussian processes to better account for correlated noise is currently being developed, which will improve mass-loss constraints (McCreery et al., in preparation).

We used nested sampling (Skilling 2004, 2006) to constrain the posterior probability distributions for  $\dot{M}$  and  $T$ . Using the `dynesty`<sup>3</sup> package (Speagle 2020), we sample across a prior volume defined by  $\mathcal{U}(3, 12.5)$  for  $\log \dot{M}$  and  $\mathcal{U}(3.35, 4.35)$  for  $\log T$ . We perform dynamic nested sampling (Higson et al. 2019) with 500 initial live points, using the ‘multi’ method (i.e. multiple ellipsoids) for bounding and the ‘unif’ method (i.e. uniformly sampling within the bounds) for sampling. Convergence is achieved when the estimated change in evidence from further sampling does not exceed  $\Delta \log \mathcal{Z} > 0.5$ . The posterior distributions that we obtained are shown in Figure 3.

We estimate an 95th-percentile upper limit of  $\dot{M} < 10^{10.03} \text{ g s}^{-1}$  and a 99.7th-percentile upper limit of  $\dot{M} < 10^{11.11} \text{ g s}^{-1}$ . The latter corresponds to a mass-loss timescale of  $M_p/\dot{M} \gtrsim 40 \text{ Gyr}$ , i.e. negligible for the planet’s evolution. The outflow temperature is weakly constrained by our non-detection, similarly to e.g. Spake et al. (2022). Outflows close to our upper limit on  $\dot{M}$  are permitted only at high temperatures  $T \gtrsim 10,000 \text{ K}$ , but at lower temperatures the constraint on  $\dot{M}$  is more stringent. We re-ran the analysis using `emcee` (Foreman-Mackey et al. 2013), and verified that the joint posterior probability distribution on  $\dot{M}$  and  $T_0$  was robust to our choice of sampling methodology.

#### 4. DISCUSSION

The non-detection of helium in LTT 9779b’s atmosphere is somewhat puzzling. It is unlikely to be due to helium ionization: while some short-period planets have reduced neutral triplet helium populations due to strong photoionization (Oklopčić 2019; Biassoni et al. 2023),

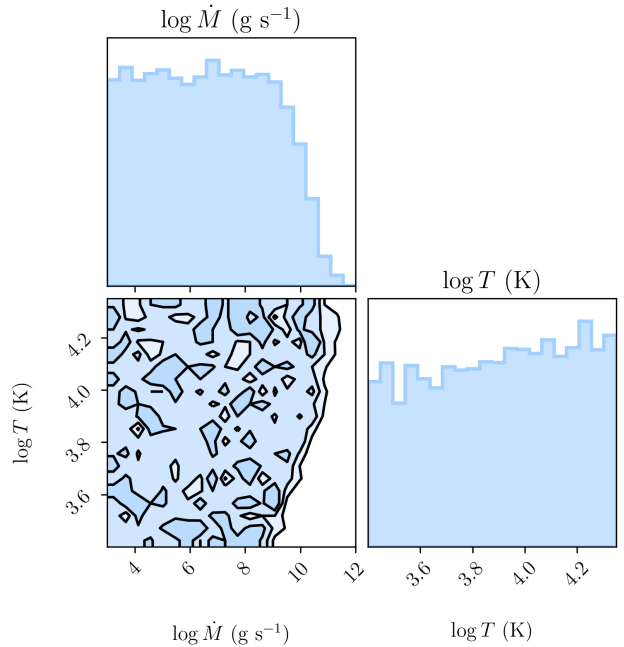


**Figure 3.** Posterior probability distributions on our sampled parameters. The plotted contours are the  $1\sigma$ ,  $2\sigma$ , and  $3\sigma$  levels for the 2D distribution.

the top-of-atmosphere XUV flux for LTT 9779b is actually quite modest. Using the Behr et al. (2023) SED, we found that LTT 9779b had a top-of-atmosphere XUV flux (integrated between  $5 \text{ \AA}$  and  $504 \text{ \AA}$ , corresponding to helium-ionizing wavelengths) of  $4800 \text{ erg s}^{-1} \text{ cm}^{-2}$ : similar to that of HD 189733b, half that of WASP-69b, and only about  $3\times$  larger than that of HAT-P-11b (Allart et al. 2023). We therefore do not expect LTT 9779b’s upper atmosphere to be substantially more ionized than these three planets, which all exhibit strong helium absorption signatures. It is more likely that either LTT 9779b’s mass-loss rate or helium abundance is low.

To determine if a low mass-loss rate is expected for this planet, we compared our upper limits ( $\dot{M} < 10^{10.03} \text{ g s}^{-1}$  at 95% confidence,  $\dot{M} < 10^{11.11} \text{ g s}^{-1}$  at 99.7% confidence) to predicted  $\dot{M}$  values from various photoevaporation models. These models require the integrated XUV flux shortward of  $912 \text{ \AA}$  (i.e. photons capable of photoionizing hydrogen and/or helium), which we estimated to be  $F_{\text{XUV}} = 6500 \text{ erg cm}^{-2} \text{ s}^{-1}$  from the MUSCLES spectrum. Using the ATES model grid from Caldiroli et al. (2022), we calculated a predicted mass-loss rate of  $\dot{M} = 7.3 \times 10^{10} \text{ g s}^{-1}$ . This is in good agreement with Edwards et al. (2023), who also used the MUSCLES spectrum from Behr et al. (2023) and predicted a mass-loss rate of  $\dot{M} \approx 10^{11} \text{ g s}^{-1}$  with a de-

<sup>3</sup> Version 2.1.2, doi: 10.5281/zenodo.3348367

tailed outflow model based on [Allan & Vidotto \(2019\)](#). These mass-loss rates are ruled out by our observations at the 95% level. Recently, [Fernández Fernández et al. \(2024\)](#) have obtained even deeper constraints on the X-ray luminosity of LTT 9779 with *XMM-Newton*. These authors estimated  $\dot{M} = 1.5 \times 10^{11} \text{ g s}^{-1}$  using the model from [Kubyshkina et al. \(2018\)](#), and  $\dot{M} = 6 \times 10^{10} \text{ g s}^{-1}$  using an energy-limited model. Both of these mass-loss rates are also ruled out by our observations at the 95% level (and the former at the 99.7% level). The discrepancy between the helium non-detection and the outflow models is more severe when we consider Roche lobe overflow, which at these distances should be greatly enhancing the outflow rate over expectations from photoevaporation alone ([Koskinen et al. 2022](#)). We conclude that the outflow rate of LTT 9779b appears to be smaller than expected, even considering the low XUV luminosity of the host star.

A number of additional factors could be playing a role in the non-detection of metastable helium. For example, outflows can be confined by the stellar wind ([Spake et al. 2021](#); [Wang & Dai 2021](#); [MacLeod & Oklopčić 2022](#)) or planetary magnetic field ([Fossati et al. 2023](#); [Schreyer et al. 2023](#)). These scenarios lead to different velocity structures of the helium triplet, but in the case of a non-detection we lack the velocity information necessary to assess these possibilities. Another assumption of our retrieval was a 90/10 H/He number ratio. If LTT 9779b’s atmosphere is substantially depleted in helium, our inferred total mass-loss rate would increase, bringing the inference into better agreement with photoevaporation models. Helium depletion has been invoked to help explain weak detections and non-detections in other systems, including the non-detection in WASP-80b ([Fossati et al. 2023](#); [Lampón et al. 2023](#)).

Our modeling has also assumed a metal-free H/He atmosphere, which a number of recent investigations call into question for LTT 9779b. Phase curve and thermal emission observations from *Spitzer*, *TESS*, and *CHEOPS* suggest that the planet is extremely reflective, with geometric albedo  $A_g = 0.80^{+0.10}_{-0.17}$  ([Crossfield et al. 2020](#); [Dragomir et al. 2020](#); [Hoyer et al. 2023](#)). [Hoyer et al. \(2023\)](#) estimated that a highly supersolar ( $> 400\times$  solar) metallicity is required for such reflective clouds to survive on the planetary dayside. These results are in some tension with [Edwards et al. \(2023\)](#), who estimate the metallicity to be sub-solar based on their *HST* WFC3 transmission spectrum. The *JWST* NIRISS/SOSS phase curves taken in Cycle 1 (GTO 1201) and planned for Cycle 2 (GO 3231) will help to resolve the discrepancy.

A high atmospheric metallicity would naturally explain the low inferred mass-loss rate for LTT 9779b. As atmospheric metallicity increases past  $100\times$  solar, the scale height of the upper atmosphere is substantially decreased and thermospheric cooling becomes dominated by metals, decreasing both the overall mass-loss rate and the He 10830 Å signal ([Owen & Jackson 2012](#); [Lopez 2017](#); [Owen & Murray-Clay 2018](#); [Ito & Ikoma 2021](#); [Nakayama et al. 2022](#); [Zhang et al. 2022](#)). Weakened evaporation due to metals may also be responsible for the non-detections of He 10830 Å in other sub-Jovian systems, including GJ 1214b ([Kasper et al. 2020](#); [Spake et al. 2022](#)), which *JWST* has revealed to be quite metal-rich ([Gao et al. 2023](#); [Kempton et al. 2023](#)). For LTT 9779b, a metal-rich envelope may be the final product of rapid atmospheric loss, which is more likely from Roche lobe overflow or partial tidal disruption than photoevaporation ([Guillochon et al. 2011](#); [Koskinen et al. 2022](#); [Vissapragada et al. 2022](#); [Osborn et al. 2023](#)). Ultra-hot Neptunes may have started their lives as gas giants before catastrophic envelope loss ensued and deeper, metal-enriched gas was exposed, making the planet resilient to further photoevaporation ([Jenkins et al. 2020](#); [Hoyer et al. 2023](#)). This might also explain why some hot Neptunes survive well into the post-main sequence evolution of their host stars ([Grunblatt et al. 2023](#)).

## 5. CONCLUSION

We observed two transits of LTT 9779b using the WINERED spectrograph on the 6.5 m Clay/Magellan II telescope. Our aim was to search for excess absorption in the metastable helium triplet during transit, which would have indicated an extended upper atmosphere. We did not detect any excess absorption: in a 0.75 Å passband centered on the helium triplet, we set upper limits of  $< 0.12\%$  ( $\delta R_p/H < 14$ ) and  $< 0.20\%$  ( $\delta R_p/H < 22$ ) at  $2\sigma$  and  $3\sigma$  respectively. Using an isothermal Parker wind model, we found the planetary mass-loss rate to be  $< 10^{10.03} \text{ g s}^{-1}$  and  $< 10^{11.11} \text{ g s}^{-1}$  at the 95th and 99.7th percentiles respectively. Our model accounted for the relatively low XUV luminosity of LTT 9779, which certainly contributes to the non-detection ([Behr et al. 2023](#); [Fernández Fernández et al. 2024](#)). Even so, our inferred mass-loss rate is at least a factor of a few smaller than predicted by photoevaporation models that assume a pure H/He composition for the planetary envelope ([Kubyshkina et al. 2018](#); [Caldiroli et al. 2022](#); [Edwards et al. 2023](#); [Fernández Fernández et al. 2024](#)).

We suggest that the non-detection of helium may be due in part to a high envelope metallicity, which has been suggested independently based on *Spitzer*, *TESS*,

and *CHEOPS* phase curve observations (Crossfield et al. 2020; Hoyer et al. 2023). Metals can efficiently cool planetary outflows, leading to smaller mass-loss rates than the pure H/He models predict. Additionally, the higher mean atomic weight of the thermosphere would depress the atmospheric scale height, making features like He 10830 Å more challenging to detect. If atmospheric metals do indeed drive weakened evaporation in planets like LTT 9779b, we expect that *JWST* will reveal a metal-rich atmosphere for this planet, and probably also for other small planets that have evaded detection in He 10830 Å (Kasper et al. 2020; Carleo et al. 2021; Spake et al. 2022; Allart et al. 2023; Guilluy et al. 2023). Conversely, if the atmospheric metallicity of LTT 9779b is not found to be significantly super-solar, the helium non-detection could be due to a low helium abundance (Lampón et al. 2023), a strong stellar wind (MacLeod & Oklopčić 2022), or the planetary magnetic field (Schreyer et al. 2023).

LTT 9779b remains one of the best desert-dwelling planets for transmission spectroscopy, and it should be prioritized for further study given the non-detection of helium escape. The *JWST* Cycle 1 NIRISS/SOSS phase curve of LTT 9779b (GTO 1201) will cover the He 10830 Å triplet wavelengths at high precision (Fu et al. 2022; Dos Santos et al. 2023). Jointly analyzing these data with the WINERED transmission spectrum will provide even stronger constraints on the helium absorption. Additionally, the H $\alpha$  line has emerged as a powerful probe of atmospheric escape in ultra-hot Jupiters (e.g. Jensen et al. 2012; Yan & Henning 2018; Wyttenbach et al. 2020; Huang et al. 2023), making it an interesting direction forward for ultra-hot Neptunes. A detection of escape in H $\alpha$  or Lyman- $\alpha$  might suggest LTT 9779b is helium-depleted rather than metal-rich (e.g. Yan et al. 2022; Lampón et al. 2023). However, Lyman- $\alpha$  spectroscopy is challenging at  $d = 81$  pc due to both the diminished stellar flux and the strong interstellar absorption. A better option in the ultraviolet may be spectroscopy of metal lines in the near-ultraviolet with *HST* (e.g. Sing et al. 2019; Linssen & Oklopčić 2023) or a future dedicated small-sat platform (France et al. 2023; Sreejith et al. 2023). If the atmospheres of ultra-hot Neptunes are indeed metal-rich, then near-UV observations may be the best way to study their upper atmospheres.

This paper is based on WINERED data gathered with the 6.5 meter Clay/Magellan II Telescope located at Las Campanas Observatory, Chile. We thank the staff at Las Campanas Observatory for their efforts to ensure a successful first science run for WINERED. In particular we thank Jorge Araya for assistance with telescope operations, and we also thank Morgan Sidel, Heather Knutson, and Yuri Beletsky for helpful conversations.

WINERED was developed by the University of Tokyo and the Laboratory of Infrared High-resolution Spectroscopy, Kyoto Sangyo University, under the financial support of KAKENHI (Nos. 16684001, 20340042, and 21840052) and the MEXT Supported Program for the Strategic Research Foundation at Private Universities (Nos. S0801061 and S1411028). The observing run in 2023 June was partly supported by KAKENHI (grant No 18H01248) and JSPS Bilateral Program Number JPJSBP120239909. A. McWilliam thanks and acknowledges receipt of a Carnegie Venture Grant, kindly provided by the Carnegie Institution for Science, in order to purchase equipment required to adapt, install and support WINERED on the Magellan Clay telescope.

*Facilities:* Magellan:Clay (WINERED spectrograph), ADS, Exoplanet Archive

*Software:* numpy (Harris et al. 2020), matplotlib (Hunter 2007), scipy (Virtanen et al. 2020), astropy (Astropy Collaboration et al. 2013, 2018), spectres (Carnall 2017), hapi (Kochanov et al. 2016), p-winds (Dos Santos et al. 2022), dynasty (Speagle 2020), emcee (Foreman-Mackey et al. 2013)



## REFERENCES

- Allan, A., & Vidotto, A. A. 2019, *MNRAS*, 490, 3760, doi: [10.1093/mnras/stz2842](https://doi.org/10.1093/mnras/stz2842)
- Allart, R., Lemée-Jolicoeur, P. B., Jaziri, A. Y., et al. 2023, arXiv e-prints, arXiv:2307.05580, doi: [10.48550/arXiv.2307.05580](https://doi.org/10.48550/arXiv.2307.05580)
- Armstrong, D. J., Lopez, T. A., Adibekyan, V., et al. 2020, *Nature*, 583, 39, doi: [10.1038/s41586-020-2421-7](https://doi.org/10.1038/s41586-020-2421-7)
- Astropy Collaboration, Robitaille, T. P., Tollerud, E. J., et al. 2013, *A&A*, 558, A33, doi: [10.1051/0004-6361/201322068](https://doi.org/10.1051/0004-6361/201322068)
- Astropy Collaboration, Price-Whelan, A. M., Sipőcz, B. M., et al. 2018, *AJ*, 156, 123, doi: [10.3847/1538-3881/aabc4f](https://doi.org/10.3847/1538-3881/aabc4f)
- Behr, P. R., France, K., Brown, A., et al. 2023, *AJ*, 166, 35, doi: [10.3847/1538-3881/acdb70](https://doi.org/10.3847/1538-3881/acdb70)
- Bennett, K. A., Redfield, S., Oklopčić, A., et al. 2023, *AJ*, 165, 264, doi: [10.3847/1538-3881/acd34b](https://doi.org/10.3847/1538-3881/acd34b)
- Biassoni, F., Caldiroli, A., Gallo, E., et al. 2023, arXiv e-prints, arXiv:2310.13052, doi: [10.48550/arXiv.2310.13052](https://doi.org/10.48550/arXiv.2310.13052)
- Caldirolì, A., Haardt, F., Gallo, E., et al. 2022, *A&A*, 663, A122, doi: [10.1051/0004-6361/202142763](https://doi.org/10.1051/0004-6361/202142763)
- Carleo, I., Youngblood, A., Redfield, S., et al. 2021, *AJ*, 161, 136, doi: [10.3847/1538-3881/abdb2f](https://doi.org/10.3847/1538-3881/abdb2f)
- Carnall, A. C. 2017, arXiv e-prints, arXiv:1705.05165, doi: [10.48550/arXiv.1705.05165](https://doi.org/10.48550/arXiv.1705.05165)
- Carter, J. A., & Winn, J. N. 2009, *ApJ*, 704, 51, doi: [10.1088/0004-637X/704/1/51](https://doi.org/10.1088/0004-637X/704/1/51)
- Crossfield, I. J. M., Dragomir, D., Cowan, N. B., et al. 2020, *ApJL*, 903, L7, doi: [10.3847/2041-8213/abb71](https://doi.org/10.3847/2041-8213/abb71)
- Delrez, L., Santerne, A., Almenara, J. M., et al. 2016, *MNRAS*, 458, 4025, doi: [10.1093/mnras/stw522](https://doi.org/10.1093/mnras/stw522)
- Dos Santos, L. A., Alam, M. K., Espinoza, N., & Vissapragada, S. 2023, *AJ*, 165, 244, doi: [10.3847/1538-3881/accf10](https://doi.org/10.3847/1538-3881/accf10)
- Dos Santos, L. A., Vidotto, A. A., Vissapragada, S., et al. 2022, *A&A*, 659, A62, doi: [10.1051/0004-6361/202142038](https://doi.org/10.1051/0004-6361/202142038)
- Dragomir, D., Crossfield, I. J. M., Benneke, B., et al. 2020, *ApJL*, 903, L6, doi: [10.3847/2041-8213/abb70](https://doi.org/10.3847/2041-8213/abb70)
- Edwards, B., Changeat, Q., Tsiaras, A., et al. 2023, arXiv e-prints, arXiv:2306.13645, doi: [10.48550/arXiv.2306.13645](https://doi.org/10.48550/arXiv.2306.13645)
- Eggleton, P. P. 1983, *ApJ*, 268, 368, doi: [10.1086/160960](https://doi.org/10.1086/160960)
- Fernández Fernández, J., Wheatley, P. J., King, G. W., & Jenkins, J. S. 2024, *MNRAS*, 527, 911, doi: [10.1093/mnras/stad3263](https://doi.org/10.1093/mnras/stad3263)
- Foreman-Mackey, D., Hogg, D. W., Lang, D., & Goodman, J. 2013, *PASP*, 125, 306, doi: [10.1086/670067](https://doi.org/10.1086/670067)
- Fossati, L., Pillitteri, I., Shaikhislamov, I. F., et al. 2023, *A&A*, 673, A37, doi: [10.1051/0004-6361/202245667](https://doi.org/10.1051/0004-6361/202245667)
- France, K., Fleming, B., Egan, A., et al. 2023, *AJ*, 165, 63, doi: [10.3847/1538-3881/aca8a2](https://doi.org/10.3847/1538-3881/aca8a2)
- Fu, G., Espinoza, N., Sing, D. K., et al. 2022, *ApJL*, 940, L35, doi: [10.3847/2041-8213/ac9977](https://doi.org/10.3847/2041-8213/ac9977)
- Gaia Collaboration, Brown, A. G. A., Vallenari, A., et al. 2021, *A&A*, 649, A1, doi: [10.1051/0004-6361/202039657](https://doi.org/10.1051/0004-6361/202039657)
- Gao, P., Piette, A. A. A., Steinrueck, M. E., et al. 2023, *ApJ*, 951, 96, doi: [10.3847/1538-4357/acd16f](https://doi.org/10.3847/1538-4357/acd16f)
- Gordon, I. E., Rothman, L. S., Hargreaves, R. J., et al. 2022, *JQSRT*, 277, 107949, doi: [10.1016/j.jqsrt.2021.107949](https://doi.org/10.1016/j.jqsrt.2021.107949)
- Grunblatt, S., Saunders, N., Huber, D., et al. 2023, arXiv e-prints, arXiv:2303.06728, doi: [10.48550/arXiv.2303.06728](https://doi.org/10.48550/arXiv.2303.06728)
- Guillochon, J., Ramirez-Ruiz, E., & Lin, D. 2011, *ApJ*, 732, 74, doi: [10.1088/0004-637X/732/2/74](https://doi.org/10.1088/0004-637X/732/2/74)
- Guilluy, G., Bourrier, V., Jaziri, Y., et al. 2023, arXiv e-prints, arXiv:2307.00967, doi: [10.48550/arXiv.2307.00967](https://doi.org/10.48550/arXiv.2307.00967)
- Harris, C. R., Millman, K. J., van der Walt, S. J., et al. 2020, *Nature*, 585, 357, doi: [10.1038/s41586-020-2649-2](https://doi.org/10.1038/s41586-020-2649-2)
- Higson, E., Handley, W., Hobson, M., & Lasenby, A. 2019, *Statistics and Computing*, 29, 891, doi: [10.1007/s11222-018-9844-0](https://doi.org/10.1007/s11222-018-9844-0)
- Hoyer, S., Jenkins, J. S., Parmentier, V., et al. 2023, *A&A*, 675, A81, doi: [10.1051/0004-6361/202346117](https://doi.org/10.1051/0004-6361/202346117)
- Huang, C., Koskinen, T., Lavvas, P., & Fossati, L. 2023, arXiv e-prints, arXiv:2304.07352, doi: [10.48550/arXiv.2304.07352](https://doi.org/10.48550/arXiv.2304.07352)
- Hunter, J. D. 2007, *Computing in Science & Engineering*, 9, 90, doi: [10.1109/MCSE.2007.55](https://doi.org/10.1109/MCSE.2007.55)
- Ikeda, Y., Kobayashi, N., Kondo, S., et al. 2016, in *Society of Photo-Optical Instrumentation Engineers (SPIE) Conference Series*, Vol. 9908, Ground-based and Airborne Instrumentation for Astronomy VI, ed. C. J. Evans, L. Simard, & H. Takami, 99085Z, doi: [10.1117/12.2230886](https://doi.org/10.1117/12.2230886)
- Ikeda, Y., Kondo, S., Otsubo, S., et al. 2022, *PASP*, 134, 015004, doi: [10.1088/1538-3873/ac1c5f](https://doi.org/10.1088/1538-3873/ac1c5f)
- Ionov, D. E., Pavlyuchenkov, Y. N., & Shematovich, V. I. 2018, *MNRAS*, 476, 5639, doi: [10.1093/mnras/sty626](https://doi.org/10.1093/mnras/sty626)
- Ito, Y., & Ikoma, M. 2021, *MNRAS*, 502, 750, doi: [10.1093/mnras/staa3962](https://doi.org/10.1093/mnras/staa3962)
- Jenkins, J. S., Díaz, M. R., Kurtovic, N. T., et al. 2020, *Nature Astronomy*, 4, 1148, doi: [10.1038/s41550-020-1142-z](https://doi.org/10.1038/s41550-020-1142-z)
- Jensen, A. G., Redfield, S., Endl, M., et al. 2012, *ApJ*, 751, 86, doi: [10.1088/0004-637X/751/2/86](https://doi.org/10.1088/0004-637X/751/2/86)

- Kasper, D., Bean, J. L., Oklopčić, A., et al. 2020, *AJ*, 160, 258, doi: [10.3847/1538-3881/abbee6](https://doi.org/10.3847/1538-3881/abbee6)
- Kempton, E. M. R., Zhang, M., Bean, J. L., et al. 2023, *Nature*, 620, 67, doi: [10.1038/s41586-023-06159-5](https://doi.org/10.1038/s41586-023-06159-5)
- Kochanov, R. V., Gordon, I. E., Rothman, L. S., et al. 2016, *JQSTRT*, 177, 15, doi: [10.1016/j.jqsrst.2016.03.005](https://doi.org/10.1016/j.jqsrst.2016.03.005)
- Koskinen, T. T., Lavvas, P., Huang, C., et al. 2022, *ApJ*, 929, 52, doi: [10.3847/1538-4357/ac4f45](https://doi.org/10.3847/1538-4357/ac4f45)
- Kubyschkina, D., Fossati, L., Erkaev, N. V., et al. 2018, *A&A*, 619, A151, doi: [10.1051/0004-6361/201833737](https://doi.org/10.1051/0004-6361/201833737)
- Kurokawa, H., & Nakamoto, T. 2014, *ApJ*, 783, 54, doi: [10.1088/0004-637X/783/1/54](https://doi.org/10.1088/0004-637X/783/1/54)
- Lampón, M., López-Puertas, M., Lara, L. M., et al. 2020, *A&A*, 636, A13, doi: [10.1051/0004-6361/201937175](https://doi.org/10.1051/0004-6361/201937175)
- Lampón, M., López-Puertas, M., Sanz-Forcada, J., et al. 2023, *A&A*, 673, A140, doi: [10.1051/0004-6361/202245649](https://doi.org/10.1051/0004-6361/202245649)
- Li, S.-L., Miller, N., Lin, D. N. C., & Fortney, J. J. 2010, *Nature*, 463, 1054, doi: [10.1038/nature08715](https://doi.org/10.1038/nature08715)
- Linsky, J. L., Fontenla, J., & France, K. 2014, *ApJ*, 780, 61, doi: [10.1088/0004-637X/780/1/61](https://doi.org/10.1088/0004-637X/780/1/61)
- Linszen, D. C., & Oklopčić, A. 2023, *A&A*, 675, A193, doi: [10.1051/0004-6361/202346583](https://doi.org/10.1051/0004-6361/202346583)
- Lopez, E. D. 2017, *MNRAS*, 472, 245, doi: [10.1093/mnras/stx1558](https://doi.org/10.1093/mnras/stx1558)
- MacLeod, M., & Oklopčić, A. 2022, *ApJ*, 926, 226, doi: [10.3847/1538-4357/ac46ce](https://doi.org/10.3847/1538-4357/ac46ce)
- Matsakos, T., & Königl, A. 2016, *ApJL*, 820, L8, doi: [10.3847/2041-8205/820/1/L8](https://doi.org/10.3847/2041-8205/820/1/L8)
- Mazeh, T., Holczer, T., & Faigler, S. 2016, *A&A*, 589, A75, doi: [10.1051/0004-6361/201528065](https://doi.org/10.1051/0004-6361/201528065)
- Nakayama, A., Ikoma, M., & Terada, N. 2022, *ApJ*, 937, 72, doi: [10.3847/1538-4357/ac86ca](https://doi.org/10.3847/1538-4357/ac86ca)
- Naponiello, L., Mancini, L., Sozzetti, A., et al. 2023, *Nature*, 622, 255, doi: [10.1038/s41586-023-06499-2](https://doi.org/10.1038/s41586-023-06499-2)
- Oklopčić, A. 2019, *ApJ*, 881, 133, doi: [10.3847/1538-4357/ab2f7f](https://doi.org/10.3847/1538-4357/ab2f7f)
- Oklopčić, A., & Hirata, C. M. 2018, *ApJL*, 855, L11, doi: [10.3847/2041-8213/aaada9](https://doi.org/10.3847/2041-8213/aaada9)
- Orell-Miquel, J., Murgas, F., Pallé, E., et al. 2022, *A&A*, 659, A55, doi: [10.1051/0004-6361/202142455](https://doi.org/10.1051/0004-6361/202142455)
- Osborn, A., Armstrong, D. J., Fernández Fernández, J., et al. 2023, arXiv e-prints, arXiv:2308.12137, doi: [10.48550/arXiv.2308.12137](https://doi.org/10.48550/arXiv.2308.12137)
- Otsubo, S., Ikeda, Y., Kobayashi, N., et al. 2016, in *Society of Photo-Optical Instrumentation Engineers (SPIE) Conference Series*, Vol. 9908, Ground-based and Airborne Instrumentation for Astronomy VI, ed. C. J. Evans, L. Simard, & H. Takami, 990879, doi: [10.1117/12.2233845](https://doi.org/10.1117/12.2233845)
- Owen, J. E., & Jackson, A. P. 2012, *MNRAS*, 425, 2931, doi: [10.1111/j.1365-2966.2012.21481.x](https://doi.org/10.1111/j.1365-2966.2012.21481.x)
- Owen, J. E., & Lai, D. 2018, *MNRAS*, 479, 5012, doi: [10.1093/mnras/sty1760](https://doi.org/10.1093/mnras/sty1760)
- Owen, J. E., & Murray-Clay, R. 2018, *MNRAS*, 480, 2206, doi: [10.1093/mnras/sty1943](https://doi.org/10.1093/mnras/sty1943)
- Persson, C. M., Georgieva, I. Y., Gandolfi, D., et al. 2022, *A&A*, 666, A184, doi: [10.1051/0004-6361/202244118](https://doi.org/10.1051/0004-6361/202244118)
- Pont, F., Zucker, S., & Queloz, D. 2006, *MNRAS*, 373, 231, doi: [10.1111/j.1365-2966.2006.11012.x](https://doi.org/10.1111/j.1365-2966.2006.11012.x)
- Rappaport, S., Sanchis-Ojeda, R., Rogers, L. A., Levine, A., & Winn, J. N. 2013, *ApJL*, 773, L15, doi: [10.1088/2041-8205/773/1/L15](https://doi.org/10.1088/2041-8205/773/1/L15)
- Salz, M., Schneider, P. C., Czesla, S., & Schmitt, J. H. M. M. 2016, *A&A*, 585, L2, doi: [10.1051/0004-6361/201527042](https://doi.org/10.1051/0004-6361/201527042)
- Schreyer, E., Owen, J. E., Spake, J. J., Bahroloom, Z., & Di Giampasquale, S. 2023, arXiv e-prints, arXiv:2302.10947, doi: [10.48550/arXiv.2302.10947](https://doi.org/10.48550/arXiv.2302.10947)
- Sing, D. K., Lavvas, P., Ballester, G. E., et al. 2019, *AJ*, 158, 91, doi: [10.3847/1538-3881/ab2986](https://doi.org/10.3847/1538-3881/ab2986)
- Skilling, J. 2004, in *American Institute of Physics Conference Series*, Vol. 735, Bayesian Inference and Maximum Entropy Methods in Science and Engineering: 24th International Workshop on Bayesian Inference and Maximum Entropy Methods in Science and Engineering, ed. R. Fischer, R. Preuss, & U. V. Toussaint, 395–405, doi: [10.1063/1.1835238](https://doi.org/10.1063/1.1835238)
- Skilling, J. 2006, *Bayesian Analysis*, 1, 833, doi: [10.1214/06-BA127](https://doi.org/10.1214/06-BA127)
- Spake, J. J., Oklopčić, A., & Hillenbrand, L. A. 2021, *AJ*, 162, 284, doi: [10.3847/1538-3881/ac178a](https://doi.org/10.3847/1538-3881/ac178a)
- Spake, J. J., Sing, D. K., Evans, T. M., et al. 2018, *Nature*, 557, 68, doi: [10.1038/s41586-018-0067-5](https://doi.org/10.1038/s41586-018-0067-5)
- Spake, J. J., Oklopčić, A., Hillenbrand, L. A., et al. 2022, *ApJL*, 939, L11, doi: [10.3847/2041-8213/ac88c9](https://doi.org/10.3847/2041-8213/ac88c9)
- Speagle, J. S. 2020, *MNRAS*, 493, 3132, doi: [10.1093/mnras/staa278](https://doi.org/10.1093/mnras/staa278)
- Sreejith, A. G., France, K., Fossati, L., et al. 2023, *ApJL*, 954, L23, doi: [10.3847/2041-8213/acef1c](https://doi.org/10.3847/2041-8213/acef1c)
- Thorngren, D. P., Lee, E. J., & Lopez, E. D. 2023, *ApJL*, 945, L36, doi: [10.3847/2041-8213/acbd35](https://doi.org/10.3847/2041-8213/acbd35)
- Virtanen, P., Gommers, R., Oliphant, T. E., et al. 2020, *Nature Methods*, 17, 261, doi: [10.1038/s41592-019-0686-2](https://doi.org/10.1038/s41592-019-0686-2)
- Vissapragada, S., Knutson, H. A., Greklek-McKeon, M., et al. 2022, *AJ*, 164, 234, doi: [10.3847/1538-3881/ac92f2](https://doi.org/10.3847/1538-3881/ac92f2)
- Wang, L., & Dai, F. 2021, *ApJ*, 914, 99, doi: [10.3847/1538-4357/abf1ed](https://doi.org/10.3847/1538-4357/abf1ed)
- Wytttenbach, A., Mollière, P., Ehrenreich, D., et al. 2020, *A&A*, 638, A87, doi: [10.1051/0004-6361/201937316](https://doi.org/10.1051/0004-6361/201937316)

- Yan, D., Seon, K.-i., Guo, J., Chen, G., & Li, L. 2022, ApJ, 936, 177, doi: [10.3847/1538-4357/ac8793](https://doi.org/10.3847/1538-4357/ac8793)
- Yan, F., & Henning, T. 2018, Nature Astronomy, 2, 714, doi: [10.1038/s41550-018-0503-3](https://doi.org/10.1038/s41550-018-0503-3)
- Youngblood, A., Pineda, J. S., Ayres, T., et al. 2022, ApJ, 926, 129, doi: [10.3847/1538-4357/ac4711](https://doi.org/10.3847/1538-4357/ac4711)
- Zhang, M., Dai, F., Bean, J. L., Knutson, H. A., & Rescigno, F. 2023, ApJL, 953, L25, doi: [10.3847/2041-8213/aced51](https://doi.org/10.3847/2041-8213/aced51)
- Zhang, M., Knutson, H. A., Wang, L., Dai, F., & Barragán, O. 2022, AJ, 163, 67, doi: [10.3847/1538-3881/ac3fa7](https://doi.org/10.3847/1538-3881/ac3fa7)
- Zhang, M., Knutson, H. A., Wang, L., et al. 2021, AJ, 161, 181, doi: [10.3847/1538-3881/abe382](https://doi.org/10.3847/1538-3881/abe382)